JOURNAL OF MAGNETIC RESONANCE **126,** 187–192 (1997)
ARTICLE NO. MN971163

# Two-Dimensional Proton Chemical-Shift Imaging of Human Muscle Metabolites*

Jiani Hu,†,‡ M. Robert Willcott,§ and Gregory J. Moore†,¶

†*Department of Radiology, Wayne State University School of Medicine, Detroit, Michigan 48201;* §*Department of Radiology, University of Texas Medical Branch, Galveston, Texas 77555; and* ¶*Department of Psychiatry and Behavioral Neurosciences, Wayne State University School of Medicine, Detroit, Michigan 48201*

Received October 15, 1996; revised March 12, 1997

**Large lipid signals and strong susceptibility gradients introduced by muscle–bone interfaces represent major technical challenges for *in vivo* proton MRS of human muscle. Here, the demonstration of two-dimensional proton chemical-shift imaging of human muscle metabolites is presented. This technique utilizes a chemical-shift-selective method for water and lipid suppression and automatic shimming for optimal homogeneity of the magnetic field. The 2D $^1$H CSI technique described facilitates the acquisition of high-spatial-resolution spectra, and allows one to acquire data from multiple muscle groups in a single experiment. A preliminary investigation utilizing this technique in healthy adult males ($n$ = 4) revealed a highly significant difference in the ratio of the creatine to trimethylamine resonance between the fast and slow twitch muscle groups examined. The technique is robust, can be implemented on a commercial scanner with relative ease, and should prove to be a useful tool for both clinical and basic investigators.** 

## INTRODUCTION

The high sensitivity and natural abundance of protons in living tissue makes them an attractive choice for magnetic resonance spectroscopy studies of human muscle. However, $^1$H MRS of human tissue presents major technical challenges (*1, 2*). The large background tissue water and lipid signals (up to five orders of magnitude larger than typical metabolite signals) must to be sufficiently suppressed if the metabolite signals are to be observed free of distortion and with an adequate signal-to-noise ratio (SNR). Another major challenge is the narrow chemical-shift range of *in vivo* $^1$H resonances. Excellent homogeneity of the magnetic field ($B_0$) is required to resolve the $^1$H peaks. Major factors in limiting the application of $^1$H CSI of skeletal muscle are the strong lipid signal and susceptibility gradients introduced by the muscle–bone and air–tissue interfaces. The combination of the strong susceptibility gradients and undesired signals can severely contaminate the desired metabolite signals. These technical problems in $^1$H MRS of the human muscle can be even more confounding in a chemical-shift-imaging (CSI) study (compared to single-voxel techniques), because the maintenance of adequate water/lipid suppression, field homogeneity, and reduction of signal contamination becomes increasingly more difficult when performing a study over a large heterogeneous volume of interest.

Due in part to these difficulties, relatively few $^1$H MRS studies have been published on human muscle (*3–15*) in comparison to large and quickly growing literature describing $^1$H MRS studies in the human brain. The limited human-muscle papers which have been published to date (*3–15*) have utilized either spectral editing or single-voxel techniques with the exception of one study (*12*) which described a 1D CSI method without lipid suppression. The limitations of the aforementioned techniques are well known. Without lipid suppression, $^1$H CSI spectra of human muscle are often severely contaminated by lipid signal from surrounding adipose tissue (such as subcutaneous fat and bone marrow). Spectral editing techniques have the advantage of reliable detection of a given metabolite (for example, lactate overlapped by a broad lipid resonance). However, by their nature, editing techniques limit the spectral information available and typically have an inherently low sensitivity. Single-voxel techniques provide a spectrum in a single given volume of interest (VOI) with relative ease of shimming and processing, but have poor sampling efficiency and have difficulty in accommodating irregularly shaped anatomy and/or pathology. In addition, postacquisition shifting of the VOI is not possible and no control or reference spectrum can be obtained at the same time to compare normal with diseased tissue (*16–18*). CSI techniques reduce these limitations by utilizing a large VOI and then subpartitioning this VOI into smaller, adjacent ''individual'' voxels. Consequently, precise *a priori* knowledge of the location and the size of the anatomy/pathology of interest is unnecessary. Spectra from multiple adjacent voxels can be used to observe

* A preliminary account of this work was presented at the Society of Magnetic Resonance Annual Meeting, Nice, France, 1995.

‡ To whom correspondence should be addressed.



1090-7807/97 $25.00

local heterogeneity, and other voxels, further from a pathologic site, can serve as internal controls. An important property unique to CSI is the ability to arbitrarily voxel-shift the localization grid in postprocessing. This makes precise and time-consuming placement of a VOI in a subject during the examination unnecessary and helps to localize the signal within a pathologic volume or desired region after the data are acquired (*19, 20*).

In this paper, we report a method for performing two-dimensional $^1$H CSI of human muscle metabolites. The technique addresses the technical difficulties inherent to $^1$H MRS in human muscle by implementing an automated shimming procedure for optimum homogeneity of the magnetic field and chemical-shift-selective suppression for background water/lipid suppression. The scheme is implemented within a 2D CSI pulse sequence and therefore has the advantages intrinsic to all CSI methods.

## MATERIAL AND METHODS

### *Chemical-Shift-Selective Technique for Water/Lipid Suppression*

Chemical-shift-selective (CHESS) pulses are commonly used for water suppression in $^1$H spectroscopy (*21, 22*). CHESS pulses suppress undesired signals by means of a selective excitation pulse applied at the water resonance frequency followed by a spoiling gradient. The main advantage of chemical-shift-selective over nonselective suppression techniques is that the former do not disturb the signals outside a defined frequency range. Chemical-shift-selective suppression techniques are also suitable to suppress background lipid signals for $^1$H MRS studies of human muscle metabolites. In particular, the intense signal from long methylene chains can be suppressed while leaving the olefinic, $\alpha$, and $\beta$ proton signals from lipid of human muscle unaffected. As described previously, lipid suppression is very important for 2D $^1$H CSI of human skeletal muscle. Unlike the human brain, lipid signals of human skeletal muscle not only come from subcutaneous tissues, but also from bone marrow, tissues between muscles, and muscle itself. Without lipid suppression, lipid contamination from adjacent fatty tissues could be severe for a small number of phase-encoding steps (*12*), and the acquisition time of a large number of phase-encoding steps for 2D CSI is often prohibitive, particularly when several averages are necessary for high spatial resolution or good spectral quality. To suppress intense signals from the long methylene chain of lipid in the human skeletal muscle without affecting desired signals, we use a Gaussian pulse with a duration of 25.6 ms and a bandwidth of 80 Hz to selectively suppress the aliphatic lipid signals. The center frequency of the lipid suppression Gaussian pulse is set at 230 Hz upfield from the water frequencies. The flip angle and interval TI (see Fig. 1) are determined empirically for each study. The flip angle is generally around 90°, and the interval TI ranges from 20 to 120 ms. It is important to choose a proper value of TI. In general, our experience has shown that a shorter TI produces better suppression efficiency. This is likely due to the multiple lipid compartments present in muscle tissue (*11*). Spoiler gradients following the Gaussian pulse are used to crush spurious signals.

### *Automated Shimming*

High $B_0$ homogeneity is required to achieve optimal spectral resolution and sensitivity and is critical for water/lipid suppression. In our experience, an automatic shimming procedure achieves better homogeneity of the magnetic field in a shorter time period than manual shimming and reproduces similar homogeneity of $B_0$ regardless of the operator. This is critically important for spectral reproducibility and quantitation. The classic approach is to maximize the energy of the free-induction decay by a method such as a simplex technique (*23*). For a large VOI, which is necessary for 2D spectroscopic imaging, it is better to use a $B_0$ map of the object of interest since the object is often heterogeneous and has large susceptibility variation. A $B_0$ map can be obtained based on phase measurements (*24–27*) or chemical-shift measurements (*28, 29*). In phase measurement, the phase of the complex reconstructed images (from two different echo times) are subtracted to yield the $B_0$ map. Phase measurements are faster than chemical-shift measurements, but may suffer if lipid signal is comparable with water, or may encounter the modulo $2\pi$ problem inherent in any phase measurement. Alternatively, chemical-shift techniques obtain a $B_0$ map by measuring the frequency of the water peak over the region of interest, avoiding the aforementioned modulo $2\pi$ and lipid/water problems. Once the $B_0$ map is measured, currents for the individual shim coils can be calculated based on their field maps.

We have previously developed a $B_0$-mapping CSI method for automatic shimming (*30, 31*). The method is described in detail in Ref. (*31*). Briefly, the automated shimming procedure minimizes the mean square root error in the magnetic field distribution measured by CSI over the region of interest, uses 12 available shim coils (all except $Z^4$), and addresses the combined water/lipid signal issue. Only one iteration was needed in 50% of cases, two in 45%, and three or more in the remainder. The mean and standard deviation of the final water linewidth from the entire volume covered by the coil were 17.0 $\pm$ 2.0 Hz. A single iteration takes 1.5 min. Like brain, human muscle is quite homogeneous. The greater linewidth observed for human muscle compared to the human brain (17.0 vs 11.7 Hz) is likely due to the short $T_2$ relaxation time (30 vs 100 ms) of water protons in human muscle (*5*). This automated shimming method has now been incorporated into our 2D CSI muscle prescan protocol.

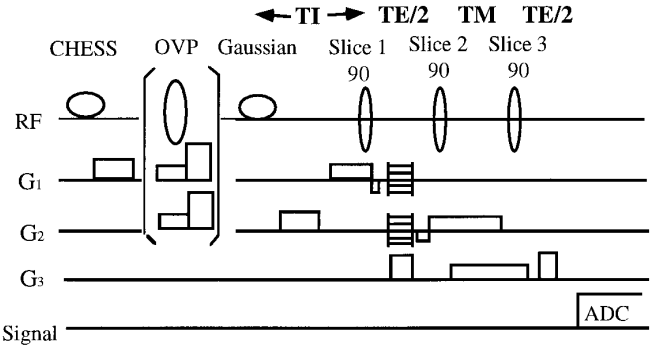


**FIG. 1.** The pulse sequence for 2D $^1$H CSI of human muscle metabolites. The technique consists of four components: water suppression (CHESS), OVP (outer volume presaturation), lipid suppression, and a standard 2D STEAM CSI sequence with TM = 10 ms, TE = 30 ms.

*Pulse Sequence*

The pulse sequence utilized for *in vivo* 2D $^1$H MRS of human muscle is shown in Fig. 1. It consists of four parts: water suppression (CHESS); outer volume presaturation (OVP); lipid suppression; and a standard 2D STEAM CSI sequence (*19, 20, 32*). Water suppression is achieved by a standard CHESS pulse sequence (*21*), using a Gaussian-shaped pulse with a bandwidth of 60 Hz and duration of 38.4 ms. OVP was accomplished by applying slice-excitation pulses to excite the area outside the volume of interest, followed by spoiler gradients (*33, 34*). Each OVP slice excitation consists of a sinc pulse with a bandwidth of 3400 Hz and a duration of 2.56 ms along with a 2 mT/m gradient in the presaturation slice direction, corresponding to a thickness of 40 mm. The presaturation directions are identical to the prelocalization directions (VOI). To deal with irregular shape of pathologic tissues, particularly these near the skin or bones, we have added the option for one additional oblique-direction presaturation pulse. Lipid suppression is achieved by a chemical-selective 25.6 ms Gaussian pulse with a bandwidth of 80 Hz. A standard 2D STEAM CSI sequence (*19, 20, 32*) has an echo time (TE) of 30 ms and a mixing time (TM) of 10 ms with 16 × 16 phase-encoding steps. The VOI over which CSI data are measured is defined by the three orthogonal slice excitations in the STEAM sequence. Each slice excitation is accomplished by a sinc pulse with duration of 5.12 ms. The gradients along the $B_0$ direction and along the two orthogonal directions are 8 and 1.5 mT/m, respectively. Typically, the VOI is 7 × 7 × 1 cm. The STEAM technique was chosen because of the familiarity of this technique and we were assured of its utility in this study. However, there are a number of alternative techniques available for VOI selection which can be used (e.g., PRESS). The combination of VOI and OVP is very helpful in reducing signal contamination, particularly if the edge of the VOI is in or near adipose tissues.

*Experimental Procedure*

All studies were performed on a clinical 1.5 whole-body imager (Siemen's 63SP, Iselin, New Jersey) using a standard linear knee coil. The following protocol was used for our *in vivo* 2D muscle studies: (1) acquire routine gradient-recalled echo images with TE = 10 ms and TR = 300 ms; (2) perform automated CSI shimming procedure; (3) determine the position and size of the VOI; (4) optimize the water suppression; (5) optimize the lipid suppression; (6) acquire 1D FID from the entire VOI; and (7) acquire 2D $^1$H CSI data set. The entire protocol is typically completed within 1 h.

Following the study, data were transferred via a network link to a UNIX workstation (Sun SPARC 20, Mountain

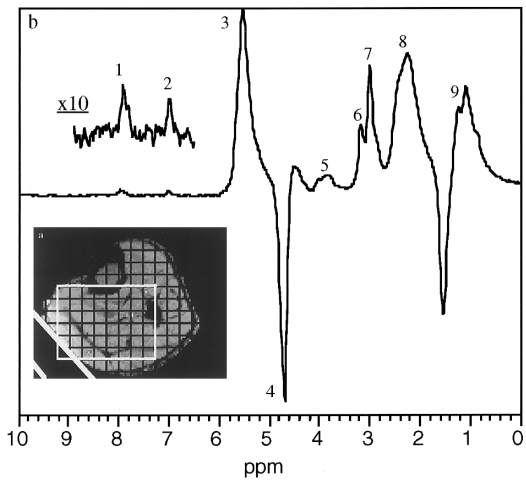


| Peak | position(ppm) | Compound |
|---|---|---|
| 1 | 8.0 | C2 of carnosine |
| 2 | 7.0 | C4 of carnosine |
| 3 | 5.4 | olefinic proton of lipid |
| 4 | 4.7 | residual water |
| 5 | 3.9 | methylene protons of Cr |
| 6 | 3.2 | TMA |
| 7 | 3.0 | Cr |
| 8 | 2.0-2.5 | α-/β- methylene of lipid |
| 9 | 0.8-1.8 | long chain methylene of lipid |

**FIG. 2.** A typical $^1$H spectrum of the middle calf muscle region from a normal healthy male volunteer using a standard linear knee coil with a TM = 10 ms, TE = 30 ms, TR = 1.0 s, and averages = 16. Resonances were assigned according to the literature (*4, 5, 15*). See text for further details.

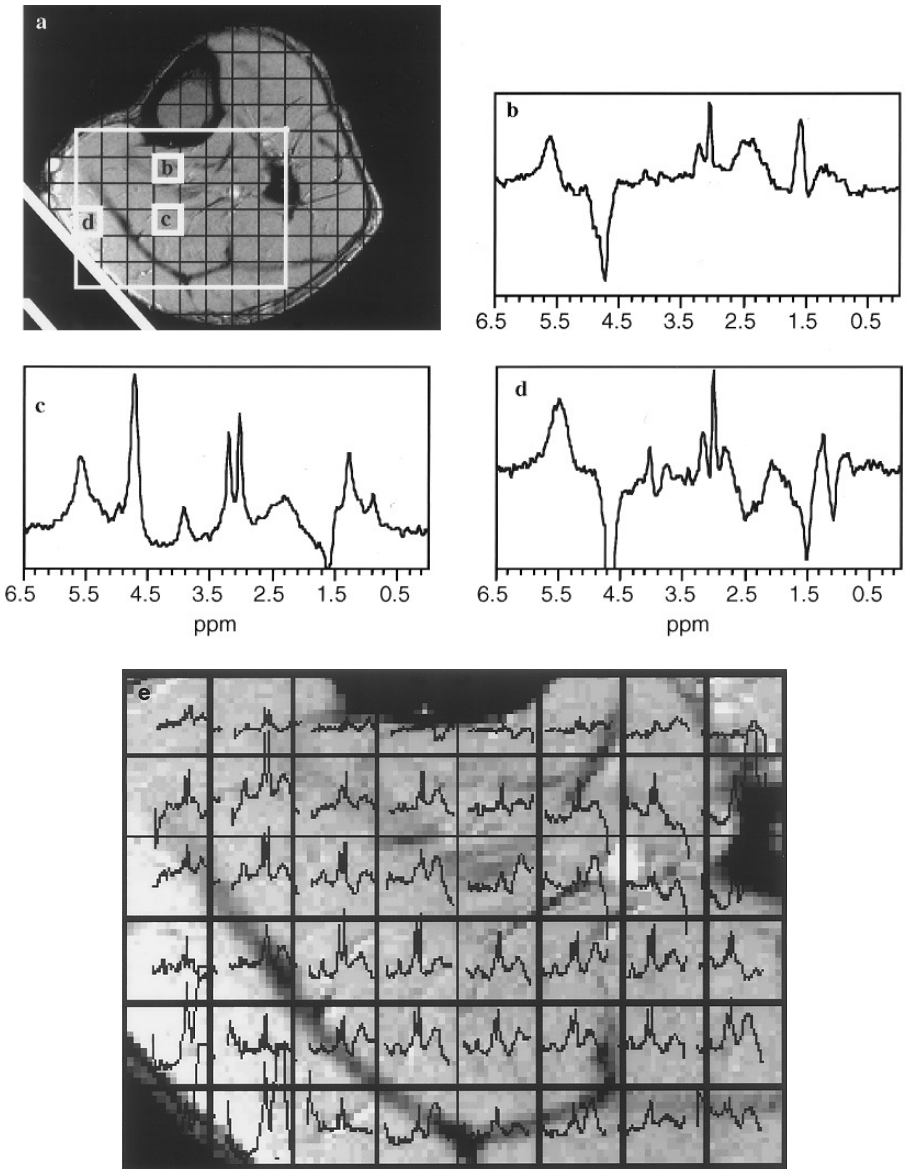


**FIG. 3.** (a) An axial MR image of the middle calf of a normal male volunteer. (b, c, d) $^1$H spectra from the tibialis posterior, soleus, and gastrocnemius muscles, respectively. (e) $^1$H CSI spectra overlaid in the zoomed image of (a). All spectra are displayed from 0 to 6.5 ppm and were acquired with the following parameters: TM = 10 ms, TE = 30 ms, TR = 1.0 s, averages = 4, thickness = 1.0 cm, a voxel size of 0.77 cm$^3$, and a total acquisition time of 17.5 min.

View, California) for off-line postprocessing. Spectral postprocessing consisted only of multiplying the individual FIDs with a 1.5 Hz exponential filter in the time domain, Fourier transformation in the temporal and two spatial dimensions, and phase correction.

## RESULTS AND DISCUSSION

Figure 2b is a typical $^1$H muscle spectrum from the VOI in the middle calf of a normal volunteer as shown in Fig. 2a. The oblique presaturation was used to suppress the subcutaneous lipid inside the rectangle box as shown in Fig. 2a. The spectrum was acquired with a repetition time (TR) of 1.0 s, 16 averages, and 1024 points. All signals were assigned according to the literature (*4*, *5*, *15*) and are noted in the table. The insert covering the aromatic range is magnified by a factor of 10. The resonances at 8.0 ppm (peak 1) and 7.0 ppm (peak 2) are from the imidazole protons (the C-2 and C-4 aromatic ring protons) of carnosine ($\beta$-Ala–His). The resonances at 5.4 ppm (peak 3), 2.0–2.5 ppm (peak 8), and 0.8–1.8 ppm (peak 9, out of phase due to suppression) are from olefinic, $\alpha$-/$\beta$-methylene, and residual

**TABLE 1**
**Ratios of Cr/TMA from Various Muscle Groups**

| | Soleus type I (slow twitch) | Gastrocnemius type II (fast twitch) | Tibialis posterior type II (fast twitch) |
|---|---|---|---|
| Cr/TMA peak heights | 0.96 ± 0.14 | 1.78 ± 0.32** | 1.68 ± 0.51* |
| Cr/TMA peak areas | 0.88 ± 0.10 | 1.30 ± 0.06*** | 1.24 ± 0.16** |

*Note.* $^1$H NMR spectral characteristics are from four young healthy male adults for the soleus, gastrocnemius, and tibialis posterior muscle groups. Ratios are reported as mean plus/minus the standard deviation for two different standard analysis methods, peak heights and peak areas. *Indicates a significant difference at $p < 0.05$ using a 2-tailed paired Students $t$ test compared to the soleus; **$p < 0.01$; ***$p < 0.001$. No significant differences were observed comparing the gastrocnemius to the tibialis posterior muscle group.

long chain methylene protons of lipid, respectively. The resonance at 4.7 ppm (peak 4) is from the residual water. The resonance at 3.2 ppm (peak 6) is from N-$(CH3)_3$ of the compound class of betains such as carnitine and cholines (TMA). The resonance at 3.0 ppm (peak 7) is from N-CH3 of creatine/phosphocreatine (Cr). The origin of the resonance at 3.9 ppm (peak 5) has recently been determined to originate from the methylene protons of Cr (*15*). As evident by Fig. 2, both the water (peak 4) and the long methylene chain of lipid (peak 9) are suppressed to about the same magnitude as the metabolites.

A $^1$H 2D-FLASH axial MR image at the mid-calf level is shown in Fig. 3a. Figures 3b–3e show the corresponding $^1$H 2D CSI spectra with a TR of 1 s and four averages. Spectra are displayed from 0–6.5 ppm. A field of view of 14 × 14 cm, slice thickness of 1.0 cm, and phase encoding of 16 × 16 resulted in a nominal voxel size of 0.77 cm$^3$. The total acquisition time was 17.5 min. The spectra in Figs. 3b, 3c, and 3d originate from the tibialis posterior, soleus, and gastrocnemius muscle, respectively. In order to better demonstrate the data-gathering efficiency of the technique, Fig. 3e shows a zoomed region of the MRI in Fig. 3a, and the corresponding $^1$H 2D CSI spectra are illustrated. Note that the spectra with strong residual lipid signals come from either subcutaneous tissue or bone marrow. In practice, each individual voxel is closely examined on the data-processing workstation. Only representative voxels are illustrated in this manuscript.

As demonstrated in Fig 3, high-quality *in vivo* $^1$H muscle spectra can be obtained with the 2D CSI method described. $^1$H NMR spectral data for the soleus, tibialis posterior, and gastrocnemius muscle groups from four young healthy male adults are summarized in Table 1. Figures 3b–3d demonstrate differing spectral patterns for each muscle type, thus supporting a recent report which suggests biochemical differences among the various muscle groups (*10*). For example, spectra from muscle groups consisting of predominately fast twitch fibers (type II) from the tibialis posterior and gastrocnemius muscle spectra (Figs. 3b and 3d, respectively) are characterized by a relatively large ratio of Cr/TMA in comparison to the soleus muscle group which consists of predominately slow twitch muscle fibers (type I) and has a spectrum characterized by a near unity ratio of Cr/TMA (see Table 1 for details). Also supporting the hypothesis of muscle-specific spectral profiles is a recent $^{31}$P NMR report which demonstrated relative differences in total phosphate content between type 1 (slow twitch) and type 2 (fast twitch) muscle fibers (*35*). Fully understanding these observations may be important for clinical and physiological studies. Further studies are underway in our laboratory to quantitatively characterize proton spectra of human muscles, and to investigate the mechanisms behind them and its correlation with muscle physiology.

Muscle lipid plays an important role as a fuel in muscle activity. However, the detailed anatomic differences among individuals and uneven distribution of lipid concentration across human limbs make lipid studies of individual muscle groups difficult. As shown by the $\alpha$-/$\beta$-methylene signal of lipid in Fig. 3e, lipid signal varies dramatically across human limbs. Studies with higher spatial resolution than the 0.77 cm$^3$ reported here will be required to separate true muscle lipids versus contaminating lipids from surrounding adipose tissues. This represents an area ripe for exploration, and new technology has already been proposed which may allow for high-resolution CSI in reasonable exam times (*36*).

Compared to single-voxel techniques, the 2D CSI technique described here should provide an improved method for quantitatively investigating the suggested differences in $^1$H NMR spectra in human muscle groups of differing fiber types. Since the fine anatomical structure of human skeletal muscles varies among subjects, and the apparent spectral profile of a voxel depends on the muscle group type as discussed above, high spatial resolution is crucial for the accurate characterization of $^1$H metabolites of individual muscle groups. The capability to voxel shift in order to eliminate partial voluming of heterogeneous tissues combined with the superior spatial resolution of the 2D CSI method makes the described scheme suitable for investigations of human muscle spectroscopic characteristics. The technique described may also be useful for a variety of other basic and clinical studies including, for example, differentiating normal muscle tissue from pathological tissue in various musculoskeletal tumors (*37–40*).

In conclusion, we have demonstrated a scheme to perform *in vivo* 2D $^1$H CSI of human muscle. The procedure is robust and can be implemented with relative ease on a standard clinical scanner. The protocol described utilizes automated shimming, optimized water/lipid suppression, and a 2D $^1$H CSI pulse sequence to facilitate the acquisition of high-spa-

tial-resolution spectra of human muscle metabolites from multiple regions in a single experiment. The technique should prove to be a useful tool for basic science and clinical studies of human muscle metabolites.

## REFERENCES


1. F. W. Howe, R. J. Maxwell, D. E. Saunders, M. M. Brown, and J. R. Griffiths, *Magn. Reson. Quart.* **9,** 31 (1993).
2. B. D. Ross, *NMR Biomed.* **4,** 47 (1991).
3. J. W. Pan, J. R. Hamm, D. L. Rothman, and R. G. Shulman, *Proc. Natl. Acad. Sci. USA* **85,** 7836 (1988).
4. R. Kreis and C. Boesch, *J. Magn. Reson. B* **104,** 189 (1994).
5. H. Bruhn, J. Frahm, M. L. Gyngell, K. D. Merboldt, W. Haenicke, and R. Sauter, *Magn. Reson. Med.* **17,** 82 (1991).
6. J. W. Pan, J. R. Hamm, H. P. Hetherington, D. L. Rothman, and R. G. Shulman. *Magn. Reson. Med.* **20,** 57 (1991).
7. P. A. Narayana, J. M. Slopis, E. F. Jackson, J. Jankovic, and I. J. Butler, *Invest. Radiol.* **26,** 58 (1991).
8. F. Schick, S. Duda, H. Durk, M. Bunse, O. Lutz, and C. D. Claussen, *Magn. Reson. Imag.* **12,** 513 (1994).
9. P. Bachert, M. E. Bellemann, G. Layer, T. Koch, W. Semmler, and W. J. Lorenz, *NMR Biomed.* **5,** 161 (1992).
10. R. Kreis, T. Pfaeffli, E. Suter, H. Hoppeler and C. Boesch, Proceedings of the Society of Magnetic Resonance, New York, p. 402, 1993.
11. F. Schick, B. Eismann, W. I. Jung, H. Bongers, M. Bunse, and O. Lutz, *Magn. Reson. Med.* **29,** 158 (1993).
12. E. F. Jackson, P. A. Narayana, and D. P. Flamig, *Magn. Reson. Imag.* **8,** 153 (1990).
13. M. Barany, P. N. Venkatasubramanian, E. Mok, I. M. Siegel, E. Abraham, A. C. Wilbur, and M. F. Mafee, *Magn. Reson. Med.* **10,** 210 (1989).
14. J. W. Pan, H. P. Hetherington, J. R. Hamm, and R. G. Shulman, *Magn. Reson. Med.* **20,** 48 (1991).
15. R. Kreis, M. Koster, M. Kamber, H. Hoppeller, and C. Boesch, *Magn. Reson. Med.* **37,** 159 (1997).
16. P. A. Bottomley, *Magn. Reson. Imaging.* **2,** 1 (1992).
17. I. Michaelis, K. D. Merboldt, H. Bruhn, W. Hanicke, D. Math, and J. Frahm, *Neuroradiology* **187,** 219 (1993).
18. M. J. Fulham, A. Bizzi, M. J. Dietz, H. H.-L. Shih, R. Raman, G. S. Sobering, J. A. Frank, A. J. Dwyer, J. R. Alger, and G. D. Chiro, *Radiology* **185,** 675 (1992).
19. T. B. Brown, B. M. Kincaid, and K. Ugurbil, *Proc. Nat. Acad. Sci. USA* **79,** 3523 (1982).
20. A. A. Maudsley and S. K. Hilal, *J. Magn. Reson.* **51,** 147 (1983).
21. A. Haase, J. Frahm, W. Hanicke, and D. Matthaei, *Phys. Med. Biol.* **30,** 341 (1985).
22. C. T. W. Moonen and P. C. M. van Zijl, *J. Magn. Reson.* **88,** 28 (1990).
23. W. W. Conover, *in* ''Topics in Carbon 13 Magnetic Resonance Spectroscopy,'' Vol. 4, Chap. 2, Wiley, New York, 1984.
24. M. G. Prammer, J. C. Haselgrove, M. Shinnar, and J. S. Leigh, *J. Magn. Reson.* **77,** 40 (1998).
25. E. Schneider and G. Glover, *Magn. Reson. Med.* **18,** 335 (1991).
26. P. Webb and A. Macovski, *Magn. Reson. Med.* **20,** 113 (1991).
27. R. Gruetter, *Magn. Reson. Med.* **29,** 804 (1993).
28. I. S. Mackenzie, E. M. Robinson, A. N. Wells, and B. Wood, *Magn. Reson. Med.* **5,** 262 (1987).
29. T. Tropp, K. A. Derby, C. Hawryszko, S. Sugiura, and H. Yamagata, *J. Magn. Reson.* **85,** 244 (1989).
30. Z. Liu, T. Javaid, and J. Hu, Proceedings of the Society of Magnetic Resonance, San Francisco, p. 1174, 1994.
31. J. Hu, T. Javaid, F. Arias-Mendoza, Z. Liu, R. McNamara, and T. R. Brown, *J. Magn. Reson. B* **108,** 213 (1995).
32. J. Frahm, H. Bruhn, M. L. Gyngell, K. D. Merboldt, W. Haenicke, and R. Sauter, *Magn. Reson. Med.* **9,** 79 (1989).
33. S. Singh, B. Rutt, and S. Napel, *J. Magn. Reson.* **90,** 313 (1990).
34. D. C. Shungu and J. D. Glickson, *Magn. Reson. Med.* **30,** 661 (1993).
35. H. Takahashi, S. Y. Kuno, S. Katsuta, H. Shimojo, K. Masuda, H. Yoskioka, I. Anno, and Y. Etai, *NMR Biomed.* **9,** 8 (1996).
36. J. Hu and J. L. Evelhoch, Proceedings of the International Society of Magnetic Resonance in Medicine, New York, p. 1223, 1996.
37. W. Negendank, *NMR Biomed.* **5,** 303 (1992).
38. J. F. Huth, J. J. Mirra, and F. R. Eilber, *Am J. Clin. Oncol.* **8,** 497 (1985).
39. R. Erlemann, J. Sciuk, A. Bosse, J. Ritter, C. R. Kusnierz-Glaz, P. E. Peters, and P. Wuisman, *Radiology,* **175,** 791 (1990).
40. B. Fletcher, S. Hanna, and L. Kun, *Magn. Reson. Imaging* **8,** 771 (1990).